Research article

Wei Liu, Jie Hu*, Lan Jiang, Ji Huang, Jiangang Lu, Jiangang Yin, Zhaoling Qiu, Hailin Liu, Chen Li, Suocheng Wang and Shaojun Wang

Formation of laser-induced periodic surface nanometric concentric ring structures on silicon surfaces through single-spot irradiation with orthogonally polarized femtosecond laser double-pulse sequences

https://doi.org/10.1515/nanoph-2020-0568
Received October 12, 2020; accepted December 15, 2020; published online January 5, 2021

Abstract: In this study, we report the formation of laser-induced periodic surface nanometric concentric ring structures on silicon surfaces through single-spot irradiation with orthogonally polarized femtosecond laser double-pulse sequences (OP pulses). The period of the ring structures is marginally smaller than the irradiated laser's wavelength, which indicates that the structures are a type of low-spatial-frequency laser-induced periodic surface structures. Regular nanometric concentric ring structures can be formed when the time delay between two subpulses is approximately 1 ps (roughly from 500 fs to 1.5 ps) and the number of laser bursts is approximately 4. The formation mechanism of the concentric ring structures is attributed to the surface wave (i.e., cylindrical wave) stimulated by OP pulses through single-spot irradiation is radially distributed. Large area of concentric ring structures eliminating anisotropy in the generation of structural colors was shown in this paper.

Keywords: cylindrical wave; femtosecond laser; LSFL; nanometric concentric ring structures; silicon.

***Corresponding author: Jie Hu**, Laser Micro/Nano Fabrication Laboratory, School of Mechanical Engineering, Beijing Institute of Technology, Beijing, 100081, P. R. China, E-mail: jiehu2@bit.edu.cn. https://orcid.org/0000-0003-1444-8802

Wei Liu, Lan Jiang, Ji Huang, Zhaoling Qiu, Hailin Liu, Chen Li, Suocheng Wang and Shaojun Wang, Laser Micro/Nano Fabrication Laboratory, School of Mechanical Engineering, Beijing Institute of Technology, Beijing, 100081, P. R. China. https://orcid.org/0000-0003-0488-1987 (L. Jiang)

Jiangang Lu and Jiangang Yin, Han's Laser Technology Centre, Shennan Ave No. 9988, Nanshan District, Shenzhen City, Guangdong Province, 518057, P. R. China

1 Introduction

Nanometric concentric ring structures have attracted considerable research interest for numerous applications, such as plasmonic lens manufacturing [1, 2], surface-enhanced Raman scattering [3, 4], laser beam shaping [5, 6] and the modulation of photonic nanojets [7]. Currently, methods such as electron-beam lithography [5, 8], focused ion beam milling [1, 4], the template-assisted method [9, 10] can be used to fabricate nanometric concentric structures with good quality. However, these methods require expensive devices and complex fabrication processes and environments.

Nowadays, femtosecond laser is widely used due to its abilities in achieving nanoscale fabrication, flexible 3D fabricating capability, and fabricating almost every material [11–15]. The use of femtosecond laser could provide a new method to fabricate nanometric concentric ring structures. Several research groups have reported on the use of femtosecond laser in the manufacture of concentric ring structures. To name a few, Ma et al. fabricated ring microstructures on the surface of Zr-based metallic glass [16]. Liu et al. fabricated concentric ring structures on the wall of ablated crater on a fused silica surface [17]. These studies used a linearly polarized femtosecond laser to form concentric ring structures; however, they had periods of several micrometers to dozens of micrometers and were not nanoscale. One of the most common types of structures fabricated by femtosecond laser is laser-induced periodic surface structures (LIPSS; in this study, we specifically refer to low-spatial-frequency LIPSS [LSFL]). The period of these structures is marginally smaller than the irradiation laser wavelength, which makes them an ideal option for fabricating nanometric concentric ring structures. LSFL are usually straight parallel periodic gratings fabricated by

using linearly polarized femtosecond laser. To form nanometric concentric ring LSFL, the polarization state of femtosecond laser should be transformed to radial polarization [18]. However, to transform a linearly polarized femtosecond laser into a radially polarized one, a complex femtosecond vector field generation system [19] or special wave plate [20] is required. In addition, the intensity distribution of the radially polarized pulse is hollow, and therefore, the ring structure does not form at the center of the irradiation area due to the very low energy there [18].

Herein, as illustrated in Figure 1(B), we introduce a new approach for fabricating laser-induced periodic surface nanometric concentric ring structures (a type of LSFL) with a period marginally smaller than the irradiated laser's wavelength on silicon surfaces. This approach involves fabricating the nanometric structures through single-spot irradiation with OP pulses. To obtain regular concentric ring structures, the time delay between two subpulses should be set to approximately 1 ps (roughly from 500 fs to 1.5 ps) and the number of laser bursts should be approximately 4. For a larger number of laser bursts, the rim of the irradiated area retains the concentric ring structures; however, the center of the irradiated area is damaged. The potential mechanism behind this phenomenon is that the surface wave (i.e., cylindrical wave) stimulated by the OP pulses through single-spot irradiation is radially distributed. LSFL can form through periodic energy deposition along the cylindrical wave direction, and radially distributed cylindrical wave result in the formation of a nanometric ring LSFL. Besides, large-area concentric ring structures that eliminate anisotropy in the generation of structural colors were fabricated.

2 Experimental setup and characterization

Figure 1(A) presents the experimental setup used in our study. A linearly polarized femtosecond laser with a central wavelength of 800 nm, pulse duration of 300 fs, and repetition rate of 10 Hz was generated by an amplified mode-locked Ti:sapphire laser system (Spectra Physics Inc.). The linearly polarized femtosecond laser beam was then transformed into OP pulses by using a Michelson interferometer with a 45° rotated quarter-wave plate placed in one of its arms. The cube-mounted pellicle beamsplitter (Thorlabs, CM1-BP145B2) was used to split the single pulse into double pulses. The energies of two subpulses were kept equal by adjusting the two attenuators placed on the two arms of the Michelson interferometer. The time delay between the OP pulses was changed by adjusting the optical path difference between two arms of the Michelson interferometer. The irradiated material was polished (1 1 1) crystalline silicon. The number of laser bursts delivered to the surface was determined by an optical beam shutter (Thorlabs). The laser was focused on the irradiated material surface through a convex lens with a focal length of 100 mm at a normal incidence. The beam diameter of laser before entering the convex lens was set to 4 mm. By using the method reported in the study by Liu [21], measuring the diameter of the ablated spot (D) as a function of the incident pulse energy (E_{in}), we can derive the on-target Gaussian spot diameter was about 38 μm and the silicon ablation threshold was approximately 0.131 J/cm^2. The morphology of the fabricated structures was examined with SEM (Hitachi S-4800, Ibraraki, Japan). Three-dimensional morphology of concentric ring structures

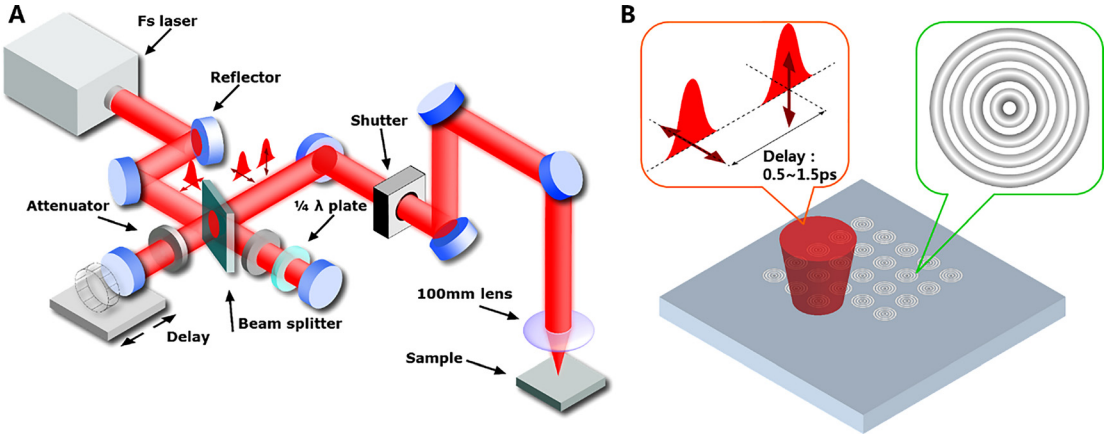

Figure 1: (A) Experimental setup based on a Michelson interferometer used in our study. (B) Illustration of the fabrication of nanometric concentric ring structures.

was characterized using an AFM (Dimension Edge PSS, Bruker, Inc., Karlsruhe, Germany).

3 Results and discussion

3.1 The relationship between the orientation and morphology of LSFL and the angle between the polarization directions of the double-pulse

Figure 2 depicts the structures by irradiating the silicon surface through single-spot irradiation with different polarized femtosecond laser double-pulse sequences. The angle between the polarization directions of the double-pulse was selected as 0°, 30°, 60° and 90°. The laser repetition was 10 Hz. The peak laser fluence of each pulse was set at 0.122 J/cm^2; this value was marginally lower than the silicon ablation threshold. As reported in the studies by Bonse and Kruger and Obona et al. [22, 23], the pulse number plays an important role in the formation of LSFL. Only several pulses of the femtosecond laser are required to form LSFL. For large pulse numbers, the LSFL still exist but are severely ablated. Therefore, we selected a pulse number of only 4 to conduct the first part of our experiment. The term "pulse number" is replaced by "burst number" to avoid confusing the number of pulses in the pulse sequence in other parts of the article. Two double-pulse time delays 0 and 1200 fs were chosen. At a time delay of 0 fs, the orientation of the LSFL was determined by the vector composition of two pulses polarizations. According to the SEM image and 2D-FFT image, when the angle was 0°, the orientation of the LSFL was exactly perpendicular to the laser polarization. When the angles were 30°, 60°, and 90°, the orientation of the LSFL tilted to approximately 15°, 30° and 45° with respect to the horizontal direction. At the time delay of 1200 fs and when the angle were 0°, 30°, and 60°, the orientation of the LSFL were similar to the situation of when time delay was 0 fs. However, when the angle was 90°, an interesting phenomenon appeared, straight parallel line-shaped LSFL transformed into concentric ring structures. This phenomenon was first reported and gave us a new strategy to fabricate nanometric concentric ring structures.

3.2 Evolution of nanometric concentric ring structures with increasing double-pulse time delay

The influence of the double-pulse time delay was first investigated. Time delays of 0, 200, 500, 800, 1000, 1200, 1500, 5000, and 10,000 fs were selected. In all experiments, the laser fluence was the same as the value above. Figure 3 depicts the evolution of nanometric concentric ring structures with increasing double-pulse time delay. As indicated by the results, nanometric concentric ring structures do not form at all double-pulse time delays. At time delays of 0 and 200 fs, according to the SEM image and 2D-FFT image, almost straight LSFL were fabricated. At the time delay of 0 fs, the LSFL orientation tilted to approximately 45° with respect to the horizontal direction. Moreover, at the time delay of 200 fs, the LSFL orientation was approximately vertical. These results are consistent with previously reported observations [24]. For time delay larger than 200 fs, in the previous work [25] reported by Höhm et al., they explored the formation of LSFL on silicon surfaces with orthogonally polarized and unequal-energy

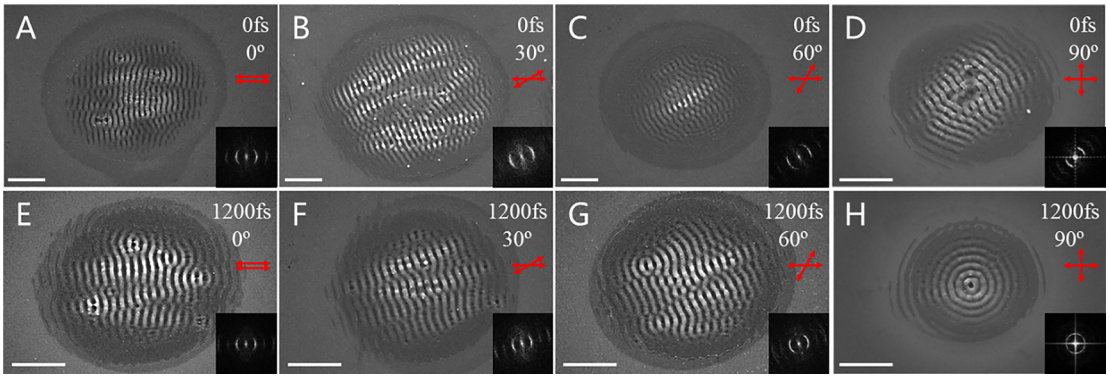

Figure 2: Formation of low-spatial-frequency LIPSS (LSFL) on silicon surfaces through single-spot irradiation with different polarized femtosecond laser double-pulse sequences. The relevant two-dimensional fast Fourier transform (2D-FFT) image is illustrated in the bottom right of each SEM image. The scale bar: represents 5 μm.

femtosecond laser double-pulse sequences. They found that the LSFL orientation of single-spot irradiation on silicon surfaces was determined by the stronger pulse and was perpendicular to its polarization. However, in our work, for time delays of 500 to 1500 fs, a new form of LSFL—nanometric concentric ring structures were formed. At the center of the irradiation area, around four to six obvious concentric rings were formed. Figure 4(A) illustrates the period as a function of the OP pulses' time delay from 0 to 1500 fs at a burst number of 4. The results indicate that in the range of 500 to 1500 fs, the period of the concentric rings as calculated by 2D-FFT was nearly constant at approximately 730 nm, which was marginally smaller than the irradiated laser's wavelength (800 nm). Thus, the periodic structures formed in this study were one type of LSFL. For time delays of 5 and 10 ps, no concentric ring structures were formed, and only some irregular structures or some nanodots were formed.

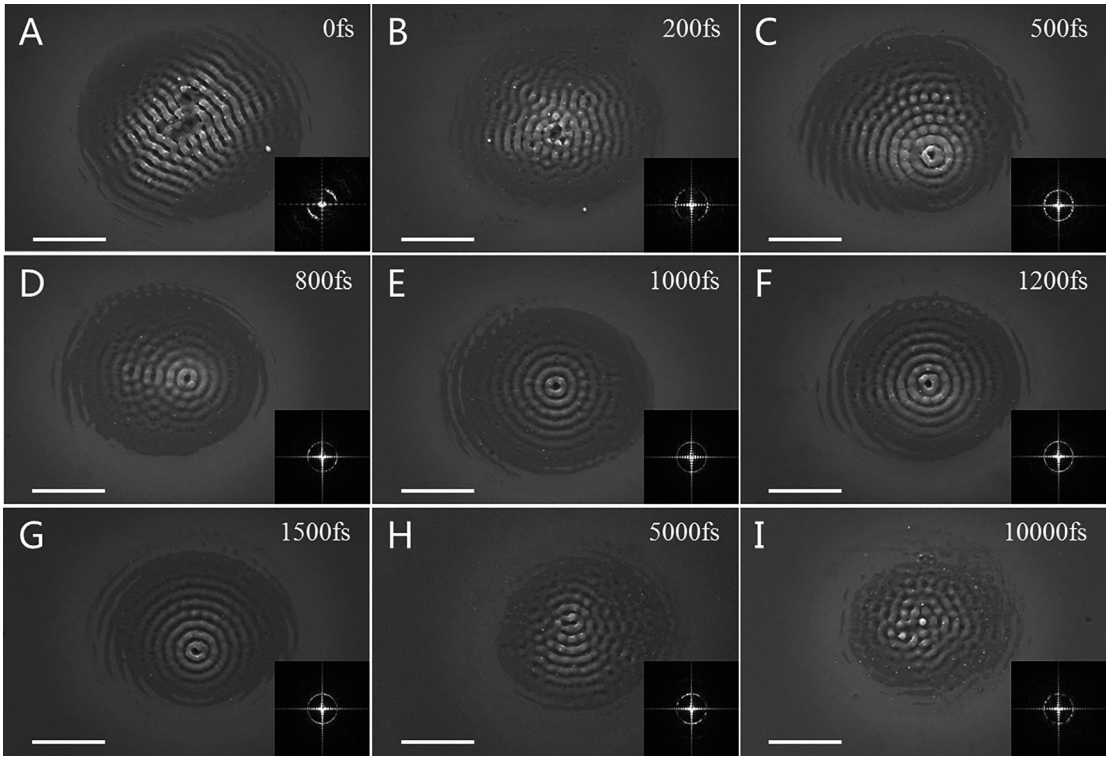

Figure 3: Formation of nanometric concentric ring structures on silicon surfaces when the burst number was fixed at 4 and the time delay was 0 fs to 10 ps. The relevant two dimensional fast Fourier transform (2D-FFT) image is illustrated in the bottom right of each SEM image. The scale bar represents 5 μm.

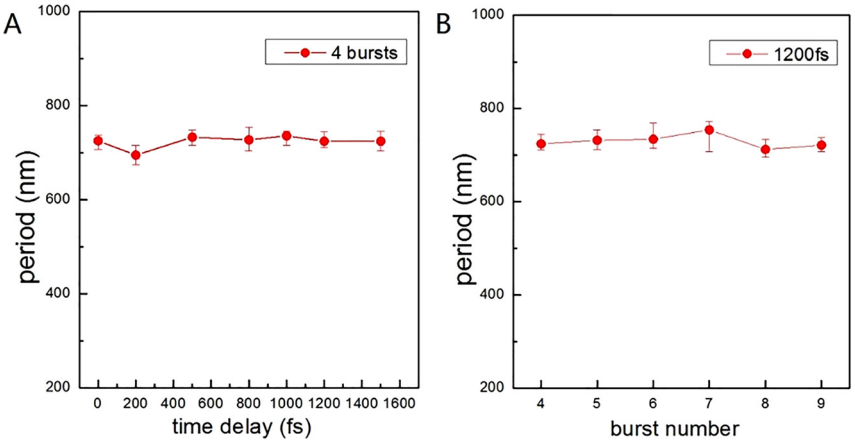

Figure 4: (A) Plot of the period of the concentric rings against the time delay at a burst number of 4. (B) Plot of the period of the concentric rings against the burst number at a double-pulse time delay of 1200 fs.

The aforementioned results indicate that concentric ring structures were formed only when the time delay between two subpulses was approximately 1 ps (roughly from 500 fs to 1.5 ps).

3.3 Evolution of nanometric concentric ring structures with increasing burst number

To study the impact of the burst number on the evolution of nanometric concentric ring structures, we selected a double-pulse time delay of 1200 fs as an example. The burst number was varied from 1 to 9. The laser repetition rate was set to 10 Hz. By controlling the opening time of optical beam shutter, we can control the number of laser bursts delivered to the surface. The silicon used in our experiments was polished and had no surface defects. Figure 5 displays images showing the evolution of nanometric concentric ring structures with an increase in the burst number. As indicated by the results, when the burst number was 1, only a modification zone was formed. When the burst number was 2 or 3, some surface defects were formed in the irradiation area. When the burst number was increased to 4, several concentric rings were formed at the center of the irradiation area due to incubation. The 2D-FFT image also verified the regularity of the formed concentric ring structures. When the burst number was increased from 5 to 9, the characteristics of the concentric rings remained unchanged. However, the concentric ring structures were gradually damaged from the center outward as the burst number increased. This observation is consistent with the situation for LSFL. LSFL are formed by a small number of laser bursts and are gradually damaged as the number of laser bursts increases. The time interval between two laser bursts was 100 ms when the laser repetition rate was 10 Hz. Because of the vibration of the fabricating platform, the irradiation spots between the adjacent laser bursts may not strictly coincide. Besides, the spatial coincidence of the two subpulses was manually adjusted. Consequently, the irradiation spots of the two subpulses may not strictly coincide. These two factors will reduce the replicability of forming concentric ring structures. The replicability of forming concentric ring structures is about 70% in our experimental conditions. Reducing the vibration of the fabricating platform and increasing the coincidence of the two subpulses help to increase the replicability of forming concentric ring structures. Figure 4(B) illustrates

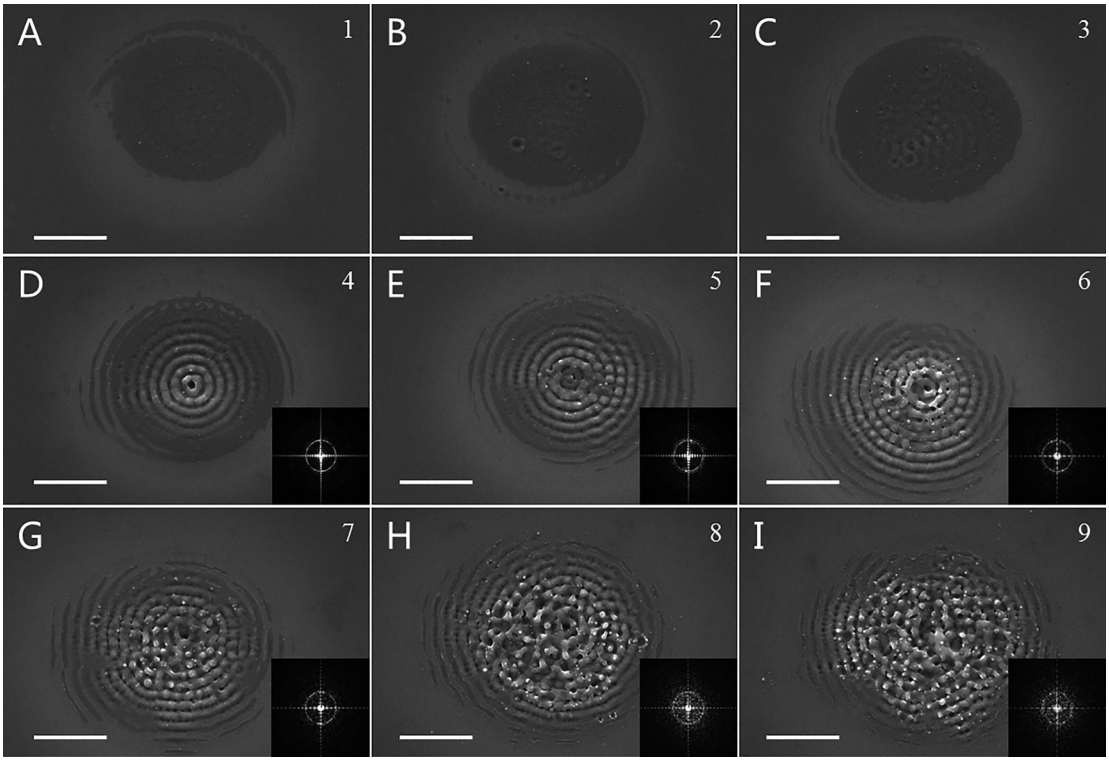

Figure 5: Formation of nanometric concentric ring structures on silicon surfaces with a burst number of 1–9 when the time delay between two subpulses was fixed at 1200 fs. Scale bar: 5 μm.

the period as a function of the burst number from 4 to 9 at a double-pulse time of 1200 fs. Similar to the situation of Figure 4(A), the period of the concentric rings was also nearly constant at approximately 730 nm.

3.4 Detailed analysis of nanometric concentric ring structures

Figure 6(A) displays a 3D perspective AFM image of concentric ring structures at the time delay of 1000 fs and burst number of 4. Four representative directions along the red, blue, green, and black lines, which are labeled as “A”, “B”, “C”, and “D”, respectively, were selected to illustrate the ablation depth of the concentric ring structures. The angle between two adjacent directions was 45°. The separate AFM profiles (ablation depth) along the red, blue, green, and black lines in Figure 6(A) are displayed in Figure 6(B). The AFM tip height is 9 μm and the opening angle of the AFM tip is about 35°. The measured depth of the central hole is about 170 nm. The half of central hole’s bottom angle is about 71°, which is significantly larger than the AFM tip angle of 35°. Therefore, the AFM tip can enter the bottom of the imprinted pattern, including the central hole. The periods of the structures along the aforementioned directions were approximately 732, 743, 703, and 743 nm, respectively. Although the periods of the structures were not strictly equal along different directions, the concentric rings were roughly circles due to the imperfect ablation conditions, such as the energy distribution of the laser pulse, spatial coincidence of the OP pulses, and vibration of the fabricating platform. Figure 6(C) depicts the combined AFM profiles (ablation depth) along the aforementioned directions. The corresponding curves of ablation depth roughly coincided.

3.5 Analysis and discussion of the formation of nanometric concentric ring structures

Although several laser-induced concentric ring structures have been reported previously, these structures cannot be classified into one class according to their period. The formation mechanism of concentric ring structures with a period of several micrometers on the surfaces, as reported by Ma et al., was attributed to the stress-induced condensation of ablation vapors and frozen thermocapillary waves on the molten surfaces [16]. The formation mechanism of concentric ring structures with a period of several microns to dozens of micrometers on the wall of an ablated crater, as reported by Liu et al., was attributed to the interference between the reflected laser field on the surface of the damaged crater and the incident laser pulse [17, 26]. The concentric ring structures in our study, which have a period marginally smaller than the wavelength of the irradiated laser, are completely different from the aforementioned two structures and are a type of LSFL. The recent works [27] by Anton Rudenko et al. put forward that the formation mechanism of LSFL is a

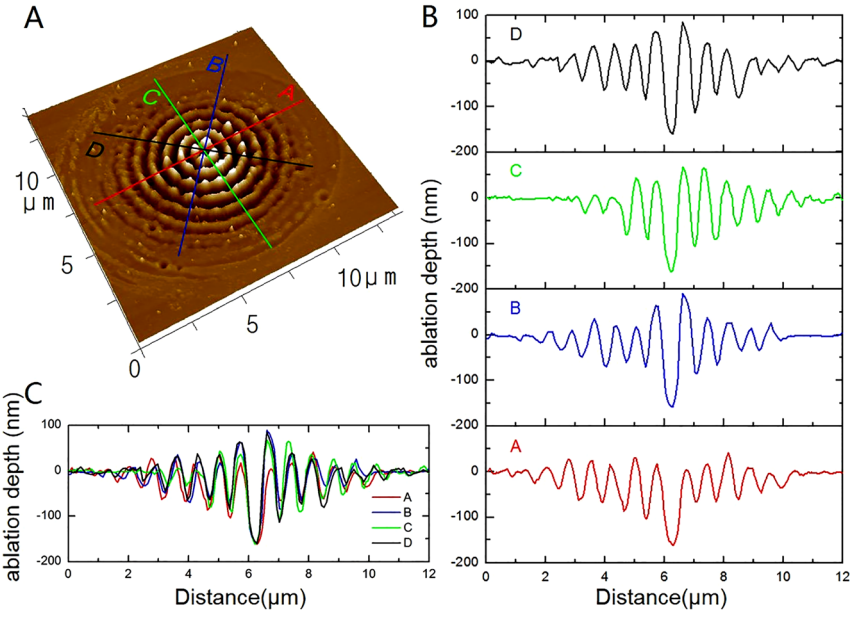

Figure 6: (A) Three-dimensional (3D) perspective AFM image of concentric ring structures at the time delay of 1000 fs and burst number of 4. (B) Separate AFM profiles (ablation depth) along the red, blue, green, and black lines in (A). (C) Combined AFM profiles (ablation depth) along the lines in (A).

process of multipulse selection of hybrid standing waves produced by the interference of the incident light with surface wave scattered by nanoholes with comparable contributions of surface plasmon polariton and cylindrical wave. For silicon, excitation of SPP requires that the silicon turns to a metallic state with the real part of permittivity $\varepsilon_r < -1$, and the free-electron density should exceed the critical density [28]. When the laser fluence is not great enough to excite the SPP, the formation of LSFL is dominant by cylindrical wave [28].

Next, we try to qualitatively clarify the conditions of obtainment of the concentric structures in the scenario of cylindrical wave considering the peak laser fluence of each pulse of OP pulses was 0.122 J/cm^2 which is not great enough to excite SPP according to the calculation in the study by Colombier et al. [28]. In most situations, the orientation of LSFL is perpendicular to the polarization of the linearly polarized femtosecond laser. Since that the direction of surface waves (SPPs, cylindrical wave) generated by linearly polarized laser is along with the direction of laser polarization [29], as the LSFL are formed by periodic energy deposition through interference between the surface waves and the incident laser, therefore, the orientation of LSFL is perpendicular to the direction of surface waves. For some special polarization states of the femtosecond laser, such as single-spot irradiation with radial and azimuthal polarized laser beams, corresponding special shape-distributed surface waves may form, and the formed structures are no longer straight parallel line structures and become periodic concentric ring structures or radial-shaped periodic structures [18].

In our experiment that involved the single-spot irradiation of OP pulses, we believe that radially distributed surface wave, i.e., cylindrical wave was formed, which may have caused the formation of concentric ring LSFL. Considering exciting surface waves at a single spot with a linearly polarized single-pulse femtosecond laser, the electric field of SPP at the observation point satisfies cos (Θ) law [30], where Θ is the angle between the direction of laser polarization and the line passing through the observation point and the center of the irradiation spot area. Although the SPP and cylindrical wave are very different by nature, the fields of cylindrical wave and SPP at the surface share many properties, such as they have nearly identical propagation constants [31]. Accordingly, we assume that the electric field of cylindrical wave at the observation point also satisfies cos (Θ) law. Herein, we propose a qualitative explanation for the formation of the concentric structures in the scenario of cylindrical wave. For single-spot irradiation with a horizontally polarized femtosecond laser beam, as depicted in Figure 7(A), point O is the center of the irradiation spot area, point R is the observation point, and θ is the angle between the direction of the horizontally polarized laser and the line passing through points O and R. At the observing point R, vector $\vec{E}_H$ means the electric field of cylindrical wave stimulated there; the orientation of the vector matches the direction of cylindrical wave (i.e., the direction of laser polarization), and the value of the vector is consistent with the amplitude of the cylindrical wave electric field. When maintaining the distance between points O and R as constant and changing the value of θ, the amplitude of the cylindrical wave electric field $|\vec{E}_H|$ can be presented as below according to the cos (Θ) law:

$$|\vec{E}_H| = E_0 \cos(\theta) \tag{1}$$

where E_0 corresponds to the maximum amplitude of the cylindrical wave stimulated by horizontally polarized femtosecond laser single-spot irradiation when θ is 0° (observation point is in the direction of laser polarization). Similarly, for vertically polarized femtosecond laser single-spot irradiation, as depicted in Figure 7(B), the amplitude of the cylindrical wave electric field $|\vec{E}_V|$ at the same observation point R, as in Figure 7(A), can be presented as below:

$$|\vec{E}_V| = E_0 \cos(\pi/2 - \theta) \tag{2}$$

By adding the vectors of cylindrical wave stimulated by horizontally polarized and vertically polarized pulses through single-spot irradiation, we can obtain the cylindrical wave stimulated by OP pulses through single-spot irradiation. As illustrated in Figure 7(C), in the direction perpendicular to the line passing through O and R, the subsequent formula can be got:

$$|\vec{E}_V|\cos(\theta) = |\vec{E}_H|\sin(\theta) \tag{3}$$

Therefore, at the observation point R, the direction of cylindrical wave stimulated by OP pulses through single-spot irradiation is exactly from the center of the irradiation spot area to the observation point. In addition, the amplitude of the cylindrical wave electric field $|\vec{E}_{CW}|$ can be obtained as below:

$$|\vec{E}_{CW}| = \sqrt{|\vec{E}_H|^2 + |\vec{E}_V|^2} = \sqrt{E_0^2\left(\cos^2(\theta) + \cos^2(\pi/2 - \theta)\right)} = E_0 \tag{4}$$

Consequently, the aforementioned equation shows that the amplitude of cylindrical wave electric field remains constant despite the different directions of the observation point if the distance between the observation point and the center of the irradiation spot remains constant. All above, as displayed in Figure 7(D), the cylindrical wave stimulated

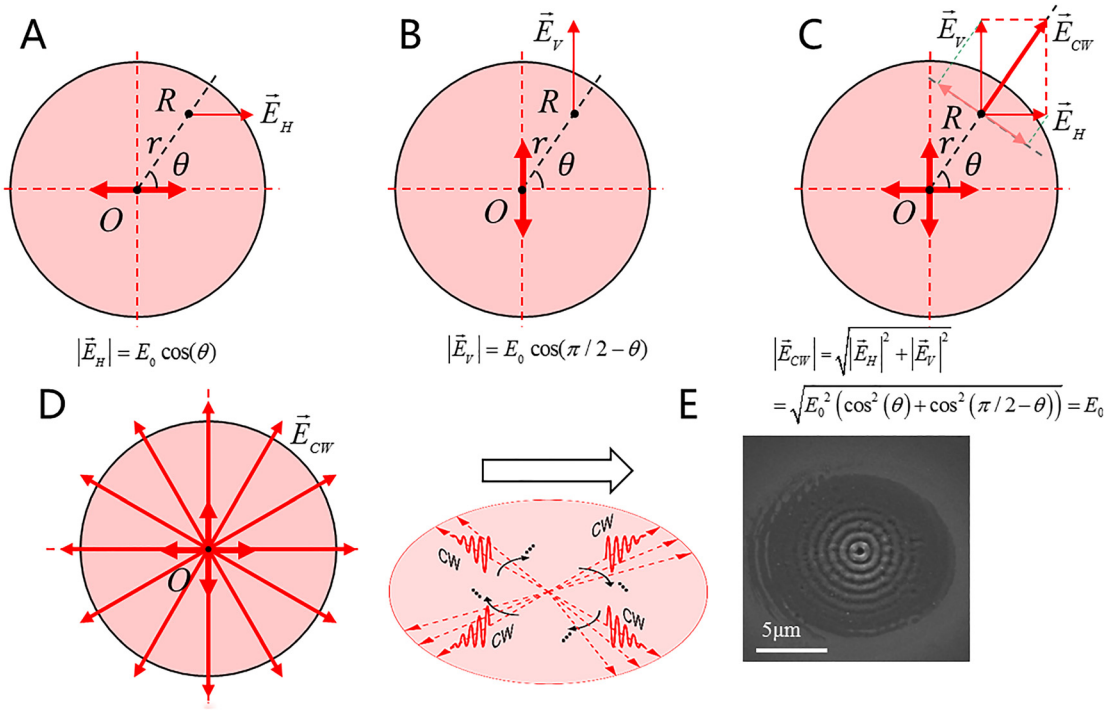

Figure 7: (A) Case of horizontally polarized femtosecond laser single-spot irradiation. (B) Case of vertically polarized femtosecond laser single-spot irradiation. (C) Case of single-spot irradiation of OP pulses. (D) Spatial distribution of cylindrical wave stimulated with OP pulses through single-spot irradiation. (E) SEM image of concentric ring structures.

by OP pulses through single-spot irradiation are radially distributed, which causes the formation of the concentric ring LSFL illustrated in Figure 7(E).

Similar to our previous work of writing the lines of periodic fringes, by scanning the silicon surfaces rather than single-spot irradiation with OP pulses, we could get the lines of periodic fringes which were always oriented perpendicular to the writing direction [32]. The time delay between the OP pulses is an important factor in this study. Concentric ring structures are not formed only when the time delay is approximately 1 ps (roughly from 500 fs to 1.5 ps). The time delay between the OP pulses should exceeds the pulse duration, but not too large. In a previous work [24] by Fraggelakis et al., they investigated the effect of the phase delay between the two incident electric fields (orthogonally polarized double-pulse femtosecond laser) on the LSFL. They irradiated the silicon surfaces choosing 6 successive time delay values with a step of 0.5 fs within a 2.5 fs delay frame. They found the orientation of LSFL rotated with the interpulse phase delay. This was because when the time delay was shorter the pulse duration, the orthogonally polarized double-pulse femtosecond laser could be seen as a single-pulse femtosecond laser with its polarization can be either elliptical, or in ideal cases linear or circular. For elliptically polarized fs-pulses, LSFL formation occurs perpendicular to the polarization ellipse's major axis. Therefore, in our work, when the time delay is shorter than the laser pulse duration, the two subpulses will interact with each other and could be seen as a single-pulse either elliptical, or in ideal cases linear or circular polarized femtosecond laser, as a result, only parallel linearly periodic grating LSFL will be formed and the concentric ring structures will not come into being, which is similar to the results reported by Fraggelakis et al. When the time delay is up to 5 ps or longer, no concentric ring structures were formed, and only some irregular structures or some nanodots were formed. For surface waves (both SPP and cylindrical wave), once the driving external radiation field is turned off (i.e., at the end of the first femtosecond laser irradiation), they may exist for a certain duration called the lifetime of the surface waves [33]. For SPP stimulated on silicon surfaces, when the wavelength of laser is 800 nm, according to the corresponding calculation by Petrakakis et al., the lifetime of SPP is about some hundreds of femtoseconds at large free electron density [34]. Another calculation by Zhang et al. reports that the SPP lifetime is no longer than 0.63 ps [35]. For cylindrical wave on silicon surfaces, there is no accurate calculation of

lifetime of cylindrical wave at present, however, the cylindrical wave decays more slowly than the SPP [36]. We can deduce that the lifetime of cylindrical wave is longer than the lifetime of SPP and may be a picosecond or several picoseconds. To form the radially distributed cylindrical wave to form the concentric ring structures, the cylindrical wave stimulated by each pulse of the orthogonally polarized femtosecond laser double-pulses should coexist for vector addition before the first one diminishes and disappears. Therefore, the time delay of the orthogonally polarized femtosecond laser double-pulses should not be too large and exceed the lifetime of cylindrical wave. All above, the time delay should exceed the pulse duration but not too large (shorter than the lifetime of cylindrical wave) and be approximately 1 ps.

3.6 Application of concentric ring structures in structural color

In general, for parallel gratings, when white light is vertically irradiated on the relevant region, the structural color can be observed in the direction perpendicular to the gratings. However, in the direction parallel to the grating, the structural color cannot be observed. This anisotropy may limit the application of parallel gratings in surface coloration. In this study, we put forward an approach for fabricating structural color surfaces by using concentric ring structures to eliminate anisotropy in the generation of structural colors. As depicted in Figure 8, we used OP pulses to fabricate a large "BIT"-shaped area formed by concentric ring structures on a 1 cm × 1 cm silicon wafer. The distance between two adjacent points was 30 μm. Figure 8(B) shows the corresponding optical microscopy image of the processing area, and the bottom-right-hand image of Figure 8(B) is an SEM image of the concentric ring structures at a single point. As the concentric ring structures have diffraction gratings in all directions, when white light was used to irradiate the processing area surface vertically, the structural colors could be observed in any directions. So next, as illustrated in Figure 8(A), at the fixed photographing position, when we rotate the silicon wafer horizontally, we can observe the structural colors at any sample rotation angle. Figure 8(C) shows the images of the structural colors at different sample rotation angles and different diffraction angles. At different diffraction angles, different wavelengths of light will be diffracted and corresponding structural color will be formed. Three representative colors of cyan (the first row), yellow (the second row) and red (the third row) were chosen for display. At fixed diffraction angle, sample rotation angles of 0°, 30°, 45°, 60°, and 90° were chosen to display. As we can see, the

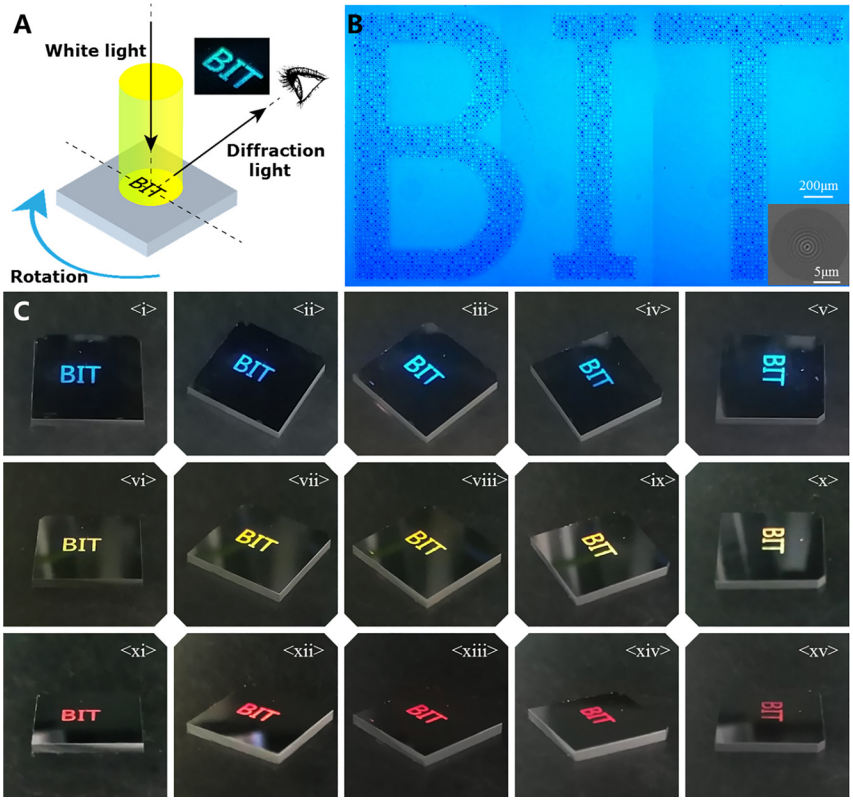

Figure 8: (A) A schematic diagram of generating structural color by vertically irradiating the processing area surface with white light. (B) Optical microscopy image of a large "BIT"-shaped area formed by concentric ring structures on a 1 cm × 1 cm silicon wafer and SEM image of a single point. (C) Images of the structural colors at different sample rotation angles and different diffraction angles.

fabricated structures exhibited structural colors independent of the sample rotation angle at the fixed photographing position and eliminated anisotropy in the generation of structural colors. The surface morphologies of the concentric ring structures provide a new method for isotropic surface functionalization.

4 Conclusion

In summary, we introduce a new method for fabricating nanometric concentric ring structures. The period of the structures was marginally smaller than the irradiated laser's wavelength, which indicated that the formed structures were a type of LSFL. When the time delay between OP pulses was set to about 1 ps (roughly from 500 fs to 1.5 ps) and the number of laser bursts was approximately 4, we obtained regular concentric ring structures. The surface wave (i.e., cylindrical wave) stimulated by OP pulses through single-spot irradiation was radially distributed, which resulted in the formation of a nanometric ring LSFL. Furthermore, the fabricated large-area concentric ring structures that eliminated anisotropy in the generation of structural colors have good application prospects.

Author contributions: All the authors have accepted responsibility for the entire content of this submitted manuscript and approved submission.
Research funding: This work has been supported by the National Key R&D Program of China (2018YFB1107200). National Natural Science Foundation of China (Grant Nos. 51675048 and 51675049).
Conflict of interest statement: The authors declare no conflicts of interest regarding this article.

References

[1] W. B. Chen, D. C. Abeysinghe, R. L. Nelson, et al., "Plasmonic lens made of multiple concentric metallic rings under radially polarized illumination," *Nano Lett.*, vol. 9, pp. 4320–4325, 2009.
[2] J. X. Ji, Y. G. Meng, L. Sun, et al., "Strong focusing of plasmonic lens with nanofinger and multiple concentric rings under radially polarized illumination," *Plasmonics*, vol. 11, pp. 23–27, 2016.
[3] D. X. Wang, T. Yang, and K. B. Crozier, "Optical antennas integrated with concentric ring gratings: electric field enhancement and directional radiation," *Opt. Express*, vol. 19, pp. 2148–2157, 2011.
[4] G. F. S. Andrade, Q. Min, R. Gordon, et al., "Surface-enhanced resonance Raman scattering on gold concentric rings: polarization dependence and intensity fluctuations," *J. Phys. Chem. C*, vol. 116, pp. 2672–2676, 2012.
[5] Z. Ghadyani, I. Vartiainen, I. Harder, et al., "Concentric ring metal grating for generating radially polarized light," *Appl. Opt.*, vol. 50, pp. 2451–2457, 2011.
[6] J. W. Zeng, J. Gao, T. S. Luk, et al., "Structuring light by concentric-ring patterned magnetic metamaterial cavities," *Nano Lett.*, vol. 15, pp. 5363–5368, 2015.
[7] M. X. Wu, B. J. Huang, R. Chen, et al., "Modulation of photonic nanojets generated by microspheres decorated with concentric rings," *Opt. Express*, vol. 23, pp. 20096–20103, 2015.
[8] N. A. Cinel, S. Cakmakyapan, G. Ertas, et al., "Concentric ring structures as efficient SERS substrates," *IEEE J. Sel. Top. Quant.*, vol. 19, p. 4601605, 2012.
[9] S. W. Hong, J. Xu, and Z. Q. Lin, "Template-assisted formation of gradient concentric gold rings," *Nano Lett.*, vol. 6, pp. 2949–2954, 2006.
[10] Y. S. Jung, W. Jung, and C. A. Ross, "Nanofabricated concentric ring structures by templated self-assembly of a diblock copolymer," *Nano Lett.*, vol. 8, pp. 2975–2981, 2008.
[11] R. R. Gattass and E. Mazur, "Femtosecond laser micromachining in transparent materials," *Nat. Photonics*, vol. 2, pp. 219–225, 2008.
[12] A. Marcinkevicius, S. Juodkazis, M. Watanabe, et al., "Femtosecond laser-assisted three-dimensional microfabrication in silica," *Opt. Lett.*, vol. 26, pp. 277–279, 2001.
[13] L. Jiang, A. D. Wang, B. Li, et al., "Electrons dynamics control by shaping femtosecond laser pulses in micro/nanofabrication: modeling, method, measurement and application," *Light Sci. Appl.*, vol. 7, 2018, https://doi.org/10.1038/lsa.2017.134.
[14] Y. Lian, L. Jiang, J. Sun, et al., "Asymmetric response optoelectronic device based on femtosecond-laser-irradiated perovskite," *ACS Appl. Mater. Interfaces*, vol. 12, pp. 17070–17076, 2020.
[15] C. Pan, L. Jiang, J. Sun, et al., "Ultrafast optical response and ablation mechanisms of molybdenum disulfide under intense femtosecond laser irradiation," *Light Sci. Appl.*, vol. 9, pp. 1–8, 2020.
[16] F. X. Ma, J. J. Yang, X. N. Zhu, et al., "Femtosecond laser-induced concentric ring microstructures on Zr-based metallic glass," *Appl. Surf. Sci.*, vol. 256, pp. 3653–3660, 2010.
[17] Y. Liu, Y. Brelet, Z. B. He, et al., "Laser-induced periodic annular surface structures on fused silica surface," *Appl. Phys. Lett.*, vol. 102, 2013, https://doi.org/10.1063/1.4812354.
[18] K. Lou, S. X. Qian, X. L. Wang, et al., "Two-dimensional microstructures induced by femtosecond vector light fields on silicon," *Opt. Express*, vol. 20, pp. 120–127, 2012.
[19] X. L. Wang, J. P. Ding, W. J. Ni, et al., "Generation of arbitrary vector beams with a spatial light modulator and a common path interferometric arrangement," *Opt. Lett.*, vol. 32, pp. 3549–3551, 2007.
[20] E. Skoulas, A. Manousaki, C. Fotakis, et al., "Biomimetic surface structuring using cylindrical vector femtosecond laser beams," *Sci. Rep.*, vol. 7, 2017, https://doi.org/10.1038/srep45114.
[21] J. Liu, "Simple technique for measurements of pulsed Gaussian-beam spot sizes," *Opt. Lett.*, vol. 7, pp. 196–198, 1982.
[22] J. Bonse and J. Kruger, "Pulse number dependence of laser-induced periodic surface structures for femtosecond laser irradiation of silicon," *J. Appl. Phys.*, vol. 108, 2010, https://doi.org/10.1063/1.3456501.

[23] J. V. Obona, J. Z. P. Skolski, G. R. B. E. Romer, et al., "Pulse-analysis-pulse investigation of femtosecond laser-induced periodic surface structures on silicon in air," *Opt. Express*, vol. 22, pp. 9254–9261, 2014.
[24] F. Fraggelakis, E. Stratakis, and P. A. Loukakos, "Control of periodic surface structures on silicon by combined temporal and polarization shaping of femtosecond laser pulses," *Appl. Surf. Sci.*, vol. 444, pp. 154–160, 2018.
[25] M. Rohloff, A. Rosenfeld, J. KrŘger, et al., "Dynamics of the formation of laser-induced periodic surface structures on dielectrics and semiconductors upon femtosecond laser pulse irradiation sequences," *Appl. Phys. A*, vol. 110, pp. 553–557, 2013.
[26] W. Sun, H. J. Qi, Z. Fang, et al., "Nanosecond laser pulse induced concentric surface structures on SiO_2 layer," *Opt. Express*, vol. 22, pp. 2948–2954, 2014.
[27] A. Rudenko, C. Mauclair, F. Garrelie, et al., "Self-organization of surfaces on the nanoscale by topography-mediated selection of quasi-cylindrical and plasmonic waves," *Nanophotonics*, vol. 8, pp. 459–465, 2019.
[28] J.-P. Colombier, A. Rudenko, E. Silaeva, et al., "Mixing periodic topographies and structural patterns on silicon surfaces mediated by ultrafast photoexcited charge carriers," *Phys. Rev. Res.*, vol. 2, p. 043080, 2020.
[29] H. Liu and P. Lalanne, "Microscopic theory of the extraordinary optical transmission," *Nature*, vol. 452, pp. 728–731, 2008.
[30] A. Drezet, A. L. Stepanov, H. Ditlbacher, et al., "Surface plasmon propagation in an elliptical corral," *Appl. Phys. Lett.*, vol. 86, 2005, https://doi.org/10.1063/1.1870107.
[31] X. Yang, H. Liu, and P. Lalanne, "Cross conversion between surface plasmon polaritons and quasicylindrical waves," *Phys. Rev. Lett.*, vol. 102, p. 153903, 2009.
[32] W. Liu, L. Jiang, W. N. Han, et al., "Manipulation of LIPSS orientation on silicon surfaces using orthogonally polarized femtosecond laser double-pulse trains," *Opt. Express*, vol. 27, pp. 9782–9793, 2019.
[33] T. J. Y. Derrien, J. Kruger, and J. Bonse, "Properties of surface plasmon polaritons on lossy materials: lifetimes, periods and excitation conditions," *J. Opt.*, vol. 18, p. 115007, 2016.
[34] E. Petrakakis, G. Tsibidis, and E. Stratakis, "Modelling of the ultrafast dynamics and surface plasmon properties of silicon upon irradiation with mid-IR femtosecond laser pulses," *Phys. Rev. B*, vol. 99, p. 195201, 2019.
[35] N. Zhang and S.-C. Chen, "Formation of nanostructures and optical analogues of massless Dirac particles via femtosecond lasers," *Opt. Express*, vol. 28, pp. 36109–36121, 2020.
[36] A. Rudenko, C. Mauclair, F. Garrelie, et al., "Light absorption by surface nanoholes and nanobumps," *Appl. Surf. Sci.*, vol. 470, pp. 228–233, 2019.